Russian Chemical Reviews **82** (7) 686 – 700 (2013) © 2013 Russian Academy of Sciences and Turpion Ltd

DOI 10.1070/RC2013v082n07ABEH004390

Cathode materials based on perovskite-like transition metal oxides for intermediate temperature solid oxide fuel cells

S Ya Istomin, E V Antipov

Contents

I.	Introduction	686
II.	Mechanism of oxygen reduction on the cathode of a solid-oxide fuel cell	688
III.	Crystal structure and properties of perovskite-like oxides	689
IV.	Thermal expansion coefficient of oxides with the perovskite structure	692
V.	Brief summary of Sections II – IV	693
VI.	Cobalt-containing perovskites	694
VII.	Nickel and copper-containing complex oxides with layered structures	696
VIII.	Conclusion	697

Abstract. The main requirements to cathode materials for intermediate temperature solid oxide fuel cells are considered with regard to the mechanism of oxygen reduction on the cathode. Factors that affect the oxide-ion and electronic conductivity and also the thermal expansion coefficient of compounds with the perovskite structure are discussed. The crystal structure, high-temperature properties and electrochemical characteristics of the most promising cathode materials based on oxygen-deficient complex oxides of cobalt and layered perovskite-like oxides of nickel and copper are analyzed. The bibliography includes 156 references.

I. Introduction

Recently, due to the constantly rising prices for traditional energy sources (coal, oil, natural gas), attention has been focused on the development of alternative power generation, particularly, hydrogen power generation built around electrochemical power sources based on fuel cells (FC). These cells convert the energy of redox reactions into the electric energy, by-passing the inefficient intermediate stage of combustion,[1–3] *e.g.*,

$$H_2 + \frac{1}{2}O_2 \longrightarrow H_2O$$

In contrast to rechargeable batteries, in fuel cells the fuel and the oxidant are constantly supplied to electrodes and the chemical reaction products are removed from them, thus providing continuous operation. The main components of all fuel cells are the cathode, the anode and the electrolyte. These elements are illustrated in Fig. 1 *a* for an individual solid oxide fuel cell (SOFC) in which hydrogen gas serves as the fuel and oxygen serves as the oxidant. On the cathode of SOFC, the oxygen reduction occurs

$$O_2(g) + 4e^- \longrightarrow 2O^{2-},$$

while on the anode, hydrogen is oxidized

$$H_2(g) + O^{2-} \longrightarrow H_2O(g) + 2e^-$$

A fuel cell battery also includes the interconnect component that provides electrical connection between the cathode of one individual fuel cell and the anode of the neighbouring cell (see Fig. 1 *b*); also, this component should prevent mixing of cathodic and anodic gases, thus preventing them from reacting with each other.

Depending on the nature of electrolyte, several main types of fuel cells are considered:[4, 5]

— alkaline cells,

— phosphoric acid cells,

— cells with a proton-exchange membrane (or with polymer electrolyte),

— cells with molten carbonate electrolyte,

— solid-oxide cells.

The main advantage of fuel cells over traditional power sources is their higher coefficient of efficiency. Fuel cells are noiseless; furthermore, when hydrogen is used as the fuel, they emit no environmentally harmful chemical compounds. Moreover, SOFC and high-temperature fuel cells (operating at temperatures >500 °C) with molten carbonate electrolytes display additional merits, namely,

— high-temperature mode makes it possible to avoid using expensive platinum metal-based catalysts;

— in high-temperature fuel cells, not only hydrogen the purity of which does not matter but also natural gas can be used as the fuel without preliminary reforming.

S Ya Istomin, E V Antipov Department of Chemistry, M V Lomonosov Moscow State University, Leninskie Gory 1, 119992 Moscow, Russian Federation. Tel. (7-495) 939 47 88,
istomin@icr.chem.msu.ru (S Ya Istomin),
evgeny.antipov@gmail.com (E V Antipov)

Received 29 March 2013
Uspekhi Khimii **82** (7) 686 – 700 (2013); translated by T Ya Safonova

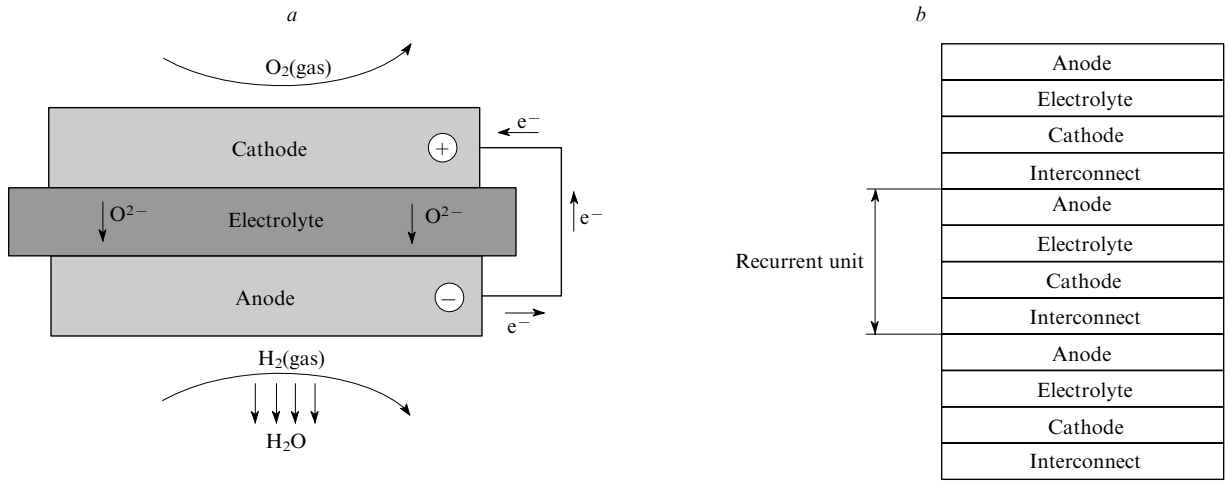


Figure 1. Schematic of an individual SOFC (*a*) and a battery of three individual fuel cells (*b*).
Standard materials of SOFC components: electrolyte, $Zr_{1-x}Y_xO_{2-x/2}$ ($x = 0.08-0.11$); cathode, $La_{1-x}Sr_xMnO_3$ ($x = 0.2-0.3$); anode, cermet-based material [60 vol.%–70 vol.% Ni(met.) + YSZ].

The state of the art in studying and designing low-temperature fuel cells and materials for them has been considered in several reviews (see, *e.g.*, Refs 6–8) and, hence, it is beyond the scope of the present review.

However, the use of high temperatures (850–1000 °C) in SOFC is a serious drawback of these electrochemical devices,[9] which still hampers their commercialization and wide use as the co-called combined heat and power sources in private houses. The main requirement to such devices is power loss not exceeding 0.1% during continuous operation for 1000 h and service life of no less than 5 years. Due to the chemical interaction of materials of SOFC components at high temperatures, its power characteristics can degrade rapidly. In high-temperature SOFC, the electrolyte represents an YSZ material based on zirconium dioxide doped with yttrium ($Zr_{1-x}Y_xO_{2-x/2}$, $x = 0.08-0.11$), the cathode represents a LSM material based on lanthanum manganite doped with strontium cations ($La_{1-x}Sr_xMnO_3$, $x = 0.2-0.3$) and the anode is made of a composite material based on cermet (metallic nickel and YSZ). Furthermore, at high temperatures, the interconnect materials for SOFC batteries should be based on oxides (for instance, doped lanthanum chromite $La_{17x}M_xCrO_3$, M = Ca, Sr),[10, 11] rather than on cheaper stainless steels. The low conductivity and the easy loss of chromium in the form of volatile compounds $Cr^{VI}O_3$ and $H_2Cr^{VI}O_4$ formed in the oxidative atmosphere in the presence of moisture[12] give rise to complications associated with the formation of chromite-based gas-tight ceramics and eventual poisoning of the SOFC surface with chromium compounds. This is why the possibility of substituting temperature-resistant steels for chromites in interconnect devices is one of the main factors that necessitate lowering the SOFC temperature down to 550–750 °C [intermediate temperature SOFC (IT-SOFC)].[13]

However, as the SOFC working temperature is lowered down, the polarization losses induced by electric current increase. The following three main types of losses are distinguished: ohmic (η_1), concentration (η_2) and activation (η_3):[14]

$$E = E_0 - \eta_1 - \eta_2 - \eta_3,$$

where E is the voltage on the working fuel cell, E_0 is the open circuit potential.

Figure 2 schematically shows the voltammogram of a working SOFC. The contributions of the mentioned types of polarization losses are shown.

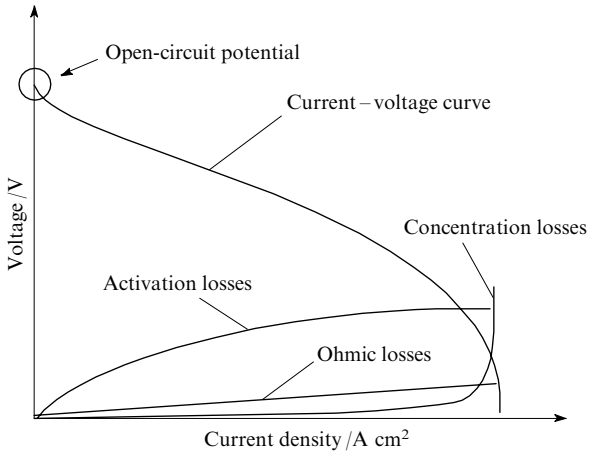


Figure 2. Current–voltage curve of a working SOFC.
Contributions made by activation, ohmic and concentration losses are marked.

Ohmic losses are associated with the electric resistance of SOFC materials, they increase with increase in the current density in accordance with Ohm's law. The reduction of ohmic losses with the rise of temperature is related to the fact that most materials of SOFC primary components exhibit conduction of the activation nature so that their resistance increases as the temperature decreases.

The concentration losses caused by the difficulties in the delivery of reactants and/or the removal of reaction products from electrodes make a considerable contribution to the total polarization only at high currents when the rates of electrochemical processes become considerable.

The activation polarization makes the largest contribution to polarization losses during SOFC operation. It appears due to complex nature of electrode redox reactions which involve several stages. Particularly, this applies to the oxygen reduction on the cathode which is accompanied by the rupture of the strong double bond in the oxygen molecule to form O^{2-} ions in vacant sites of the solid oxide.

Lowering down the temperature has a substantial effect on the activation polarization, which increases due to slowing down of electrochemical reactions on electrodes. The activation losses on the cathode exceed the losses on the anode (Fig. 3). For instance, a decrease of the SOFC working temperature from 1000 to 500 °C induces more than 2000-fold increase in the polarization resistance of the standard LSM cathode material;[15] hence, its use in IT-SOFC is out of question. A material is required that would exhibit substantially higher electrochemical activity with respect to oxygen reduction under these conditions and combine high electronic and the high oxide-ion conductivity.

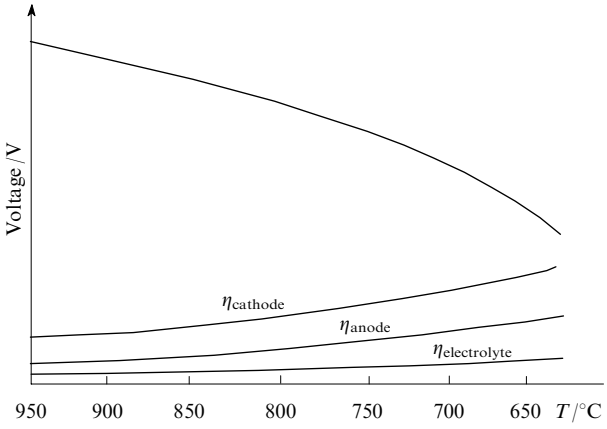


Figure 3. Temperature dependence of the voltage on a single fuel cell.
The growth of polarization losses in the electrolyte and on the cathode and anode following decrease in temperature is schematic ally shown.

Yet another problem associated with SOFC operation at high temperature is the necessity of matching the thermal expansion coefficients (TEC) of adjacent elements in fuel cells. Considerable difference in the TEC of these components leads to degradation of the cathode/electrolyte interface; the degradation becomes considerable both during the interface formation at high temperature and when the SOFC is brought to its operating mode and also at temperature cycling.

Based on the literature data, the following requirements to the cathode material of IT-SOFC can be formulated:

— high electrocatalytic activity towards oxygen reduction;

— matching of TECs of the cathode and electrolyte materials;

— the absence of chemical reaction between the electrolyte and cathode materials, which otherwise might afford a new phase capable of inhibiting the transport of charge carriers;

— stability in the cathodic gas atmosphere.

Recently, many reviews written by foreign authors have appeared which deal with the development of new materials for IT-SOFC (*e.g.*, see Refs 15–24). The present review concentrates on the chemical and structural aspects of selecting the cathode materials because this is crucial for SOFC performance and durability. According to the electronic database Scopus, in the last decade alone, more than 4000 original publications were devoted to cathode materials for SOFC. Naturally, in the present review we could not cover all information on this problem and focused attention on the description of our own studies on designing new cathode materials for SOFC and also on understanding the structure of materials studied, which determined the choice of references and also the framework of the review. The mechanism of oxygen reduction on the SOFC cathode is briefly discussed and the necessity of high oxide-ion conductivity for materials of IT-SOFC is inferred. The electronic and oxide-ion conductivities of oxides with the perovskite structure are analyzed, which is important for the practical application as SOFC materials, and the problem associated with selecting TEC is discussed.

II. Mechanism of oxygen reduction on the cathode of a solid-oxide fuel cell

The oxygen reduction on the surface of an oxide material follows a complex, multistep mechanism; the process often takes several parallel routes. The realization of one or another route substantially depends on the chemical composition, the crystal structure and the nature of charge carriers in the cathode material and also on its microstructure.

The overall equation of the reduction of oxygen molecules on the oxide surface followed by incorporation of O^{2-} ions into lattice vacancies can be described as follows (Kröger–Vink notations):

$$0.5\,O_2(g) + V_O^{\bullet\bullet} \longrightarrow O_O^x + 2h^{\bullet} \quad (1)$$

The main steps of this complex process are as follows:[14]

— adsorption of oxygen molecules on the surface of electrocatalysts (cathode material or electrolyte):

$$0.5\,O_2(g) \longrightarrow 0.5\,O_2(ad) \quad (2)$$

— dissociation of adsorbed molecules into atoms

$$0.5\,O_2(ad) \longrightarrow O(ad) \quad (3)$$

— reduction of oxygen to O^{2-} ions followed by their incorporation into vacant sites in the oxide lattice

$$O(ad) + 2e^- + V_O^{\bullet\bullet} \longrightarrow O_O^x \quad (4)$$

Depending on the nature of cathode material, the last step can occur either on the cathode surface if the material exhibits mixed (electronic and oxide-ion) conductivity or on the three-phase boundary if the oxide-ion conductivity of the cathode material is negligible (see the left and right sides of Fig. 4, respectively). The latter case corresponds to the standard cathode material used in LSM-based high-temperature SOFC. The three-phase boundary represents the space where the cathode material, the gas phase and the electrolyte are in contact. If the adsorbed oxygen atoms are

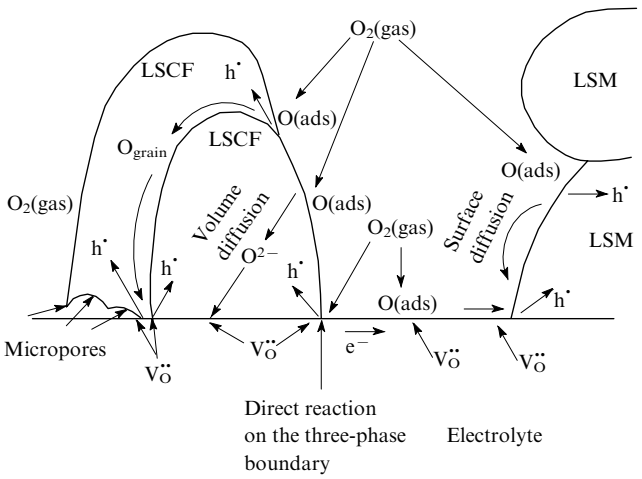


Figure 4. Possible paths of oxygen reduction on a porous cathode in SOFC.[14]
The left side of the figure corresponds to the case of oxygen reduction on the particles of a cathode material with mixed electronic and oxide-ion conductivity (*e.g.*, $La_{1-x}Sr_xCo_{1-y}Fe_yO_{3-\delta}$), the right side corresponds to oxygen reduction on a cathode with negligible oxide-ion conductivity ($La_{0.8}Sr_{0.2}MnO_3$, LSM); O_{grain} is oxygen on the grain boundary.

reduced on the three-phase boundary, the process may be preceded by their diffusion to this boundary over the surface of either cathode material or electrolyte (see Fig. 4). At the oxygen reduction on the surface of a cathode material with mixed conductivity, the ions formed are incorporated into the cathode material and then they are carried to the cathode/electrolyte interface.

For cathode materials with negligible oxide-ion conductivity (*e.g.*, LSM), the cathodic reaction rate, which determines the activation polarization, and also the corresponding resistance of the cathode/electrolyte interface (R_η) depend on the length of the three-phase boundary. To reach a reasonable R_η value ($\sim 0.2\ \Omega\ cm^2$), it is necessary to decrease the LSM particle size down to <0.1 μm.[14] This is difficult for porous ceramic materials that operate at high temperatures. However, this problem can be solved by switching to cathode materials on which oxygen can be reduced at a certain distance from the cathode/electrolyte interface, namely, on the surface of particles of the cathode material, which corresponds to the aforementioned mechanism of oxygen reduction on the surface of oxides with mixed conduction.

Within the framework of the Adler–Lane–Steele model, the resistance R_η of a cathode material with mixed conductivity can be related directly to its characteristics.[25] According to this model, for a heterogeneous chemical reaction at the gas/electrode interface,

$$R_\eta = \frac{RT}{2F^2}\sqrt{\frac{\tau}{(1-\varepsilon)a\,c_O^2 D k'}} \qquad (5)$$

where F is the Faraday constant, τ, ε, a are the parameters of electrode geometry, namely, the pore tortuosity, porosity and volume-normalized surface area, respectively; c_O is the concentration of oxygen vacancies, D is the oxygen self-diffusion coefficient, k' is the oxygen surface exchange coefficient.

By using the Adler–Lane–Steele model for mixed conductors, it is possible to assess the suitability of an oxide material as the SOFC cathode based on the parameters directly related to its chemical composition and crystal structure, namely, the coefficients of self-diffusion of oxygen ions and their surface exchange. These values can be compared with coefficients (D^* and k, respectively) found experimentally for the ^{18}O isotope label by secondary-ion mass spectrometry on gas-tight ceramic samples preliminarily annealed in the $^{18}O_2$ atmosphere.[26–33]

The D^* and k values suitable for a SOFC cathode material were estimated.[34] Assuming that $R_\eta = 0.1\ \Omega\ cm^2$ and substituting the typical parameters of the cathode material microstructure into Eqn (5) showed that the D^*k product should be of the order of magnitude of 10^{-14}. Bearing in mind that the surface exchange coefficient at the working temperatures of SOFC should not exceed 10^{-6} cm s^{-1}, the D^* value for the cathode material should not be lower than 10^{-8} cm^2 s^{-1}. Table 1 presents the values of D^* and k for some complex oxides. It should be noted that the majority of compounds shown in Table 1 contain 3d transition metal cations, namely, Mn, Fe, Co, Ni and Cu, and have the structure of perovskite (ABO_3) or its derivatives. Perovskite-like oxides of cobalt, nickel and copper exhibit high D^* and k values and can be considered as promising cathode materials for IT-SOFC.

Table 1. Diffusion and surface exchange coefficients for various oxides determined by secondary-ion mass spectrometry.

Compound	D^* /cm^2 s^{-1}	k /cm s^{-1}	D^*k /cm^3 s^{-2}	T /°C	Ref.
$La_{0.65}Sr_{0.35}MnO_3$	4.0×10^{-14}	5.0×10^{-8}	2×10^{-21}	900	26
$La_{0.9}Sr_{0.1}FeO_{3-\delta}$	8.51×10^{-10}	2.92×10^{-8}	2.48×10^{-17}	850	27
$La_{0.8}Sr_{0.2}CoO_{3-\delta}$	2.0×10^{-8}	5.0×10^{-6}	1.0×10^{-13}	800	26
$Sr_{0.75}Y_{0.25}CoO_{2.62}$	1.03×10^{-8}	1.6×10^{-5}	1.65×10^{-13}	800	28
$La_2NiO_{4+\delta}$	1.71×10^{-7}	2.55×10^{-6}	4.36×10^{-13}	799	29
La_2CuO_4	$\sim1\times10^{-8}$	$\sim1\times10^{-6}$	1.0×10^{-14}	700	30
Pr_2CuO_4	7.2×10^{-13}	1.2×10^{-8}	8.6×10^{-21}	700	31

III. Crystal structure and properties of perovskite-like oxides

1. Crystal structure of perovskite

Among complex oxides containing transition metal cations, those with the perovskite structure ABO_3 prevail (Fig. 5). The perovskite structure incorporates A- and B-cations with different crystal-chemical characteristics, the chemical composition of this phase can be varied over wide limits and, correspondingly, its properties can be deliberately changed. The cations of alkali, alkaline earth and rare earth metals (REM) and also Group 13–15, Period 6 elements, namely, Tl^+, Pb^{2+} or Bi^{3+}, can function as A-cations. Large A-cations have sizes comparable with the size of O^{2-} ion. Due to this, the perovskite structure can be considered as the cubic close-packing formed by cations A and oxygen ions. In this structure, a part of octahedral voids (1/4 of their total number), which are formed solely by oxygen ions, are occupied by B-cations.[35,36] It should be noted that the perovskite crystal structure lacks positions for additional

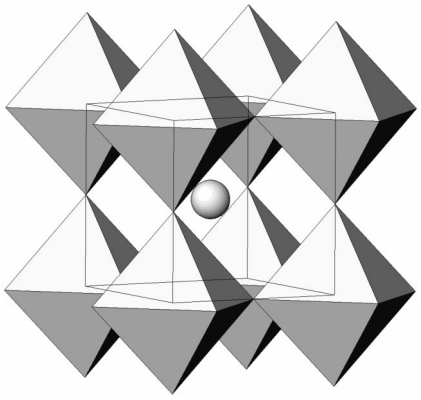


Figure 5. Crystal structure of 'ideal' cubic perovskite ABO_3. A-Cations are located at the centre of the cube and have C.N. 12, B-cations reside at cube vertices (at the centres of octahedra) and have C.N. 6. Oxygen atoms are at the corners of the octahedra.

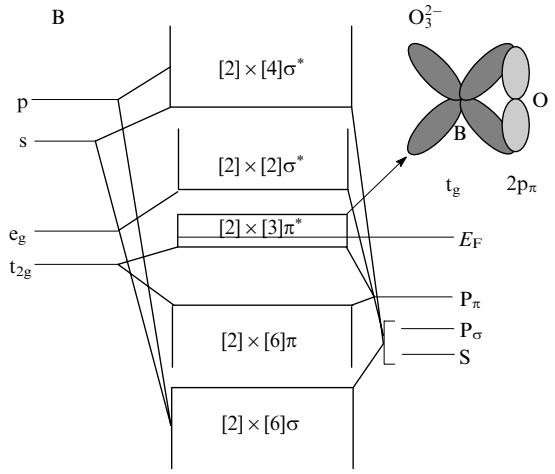


Figure 6. Model of the band structure of the perovskite ABO_3.[43] In the top right angle, the superposition of t_{2g}-orbitals of B-cation and $2p_\pi$-orbitals of oxygen to form the π*-band is shown. Bands formed with participation of A-cation are omitted. The position of the Fermi level (E_F) is shown for the case where B-cation has two valence d-electrons (the π*-band is populated by 1/3).

oxygen ions or cations. Thus, the lanthanum manganite composition written as $LaMnO_{3+\delta}$ does not imply the presence of additional oxygen ions (δ) but reflects the fact that lanthanum manganite, $La_{1-(\delta/(3+\delta))}Mn_{1-(\delta/(3+\delta))}O_3$, contains equal numbers of cation vacancies in the lanthanum and manganese sublattices.[37]

Based on the ionic model of the perovskite crystal structure, Goldschmidt[38] has derived a relationship between the ionic radii of A- and B-cations and oxygen (r_A, r_B and r_O, respectively)

$$t = \frac{r_A + r_O}{\sqrt{2}(r_B + r_O)}$$

where t is the tolerance factor equal to 1.0 for the ideal perovskite structure. However, the perovskite structure is also stable at $t < 1$, which means the presence of A-cations with the ionic radius smaller than required. In this case, the coordination number (C.N.) of the cation in A-position decreases due to cooperative rotation of the BO_6 octahedra as a result of which some of oxygen atoms move to non-bonding distances from A-cation . This gives rise to various distortions of the perovskite structure.[39–42]

2. Electronic conduction in perovskites

By varying the degree of distortion of the perovskite structure due to partial substitution of cations in A or B sublattices, it is possible to change the electronic properties of materials. As a result of interaction between d- orbitals of the transition metal and 2p-orbitals of oxygen, wide energy bands are formed (Fig. 6);[43] hence, perovskite-like oxides containing transition metal cations with partially occupied d-orbitals can exhibit high electronic conductivity. The most effective overlap of orbitals is attained for cubic perovskite, whereas for perovskites with the structure distorted due to rotation of octahedra the degree of overlap decreases. This narrows down the bands and may result in localization of electronic states and appearance of dielectric properties.

A bright illustration of the effect of the degree of structure distortion on the conductivity is the dependence of the metal–semiconductor transition temperature in $RNiO_3$ perovskites on the type of REM (R). In these phases, as the radius of the REM cation decreases and, correspondingly, the perovskite structure is distorted, the temperature of the transition to the metallic conduction state was found to increase from 135 (Pr) to 403 K (Sm).[44] This means that among RBO_3 perovskites, the highest conductivity should belong to oxides with the large REM cations: La, Ce and Pr. The typical oxidation states of the two last-mentioned elements are +3 and +4. Compounds containing Pr^{3+} are sufficiently stable, whereas those containing Ce^{3+} are unstable in the oxidative atmosphere. It should be noted that the energy of f-orbitals of praseodymium is close to the energy of 2p-orbitals of oxygen; hence, the formation of partially occupied bands and the appearance of high conductivity of praseodymium-containing perovskites are possible.

When selecting the cathode material based on perovskite-like transition-metal oxides, the trend in the variation the oxidation state of these elements should be taken into account. The stability of higher oxidation states is known to increase on going from 3d- to 4d- and 5d-elements and to be maximum for metals in the beginning of a row in the Periodic Table. This means that perovskites with high conductivity that contain cations of 4d- and 5d-elements in lower oxidation states (*e.g.*, niobium or tungsten bronzes) and also 3d-elements of the beginning of rows (*e.g.*, $LaTiO_3$ or $SrVO_3$) are unstable in the oxidative atmosphere of cathode gases. In contrast, $LaMO_3$ perovskites, where M = Cr, Mn, Fe, Co and Ni, exhibit p-type conductivity and are stable in the oxidative atmosphere in a wide temperature range. Among them, the highest conductivity is demonstrated by oxides containing manganese, cobalt or nickel. Thus, perovskites with these 3d-elements are most suitable as the cathode materials of SOFC because they are stable in the oxidative atmosphere of cathode gases and exhibit sufficiently high conductivity. The conductivity of these perovskites can be enhanced by increasing the concentration of charge carriers (holes) due to heterovalent substitution of alkaline-earth cations M^{2+} = Ca, Sr or Ba for La^{3+} (Ref 45). The data in Table 2 indicate that in some

Table 2. Total electrical conductivity (σ) of oxides $LaMO_3$ and $La_{0.7}Sr_{0.3}MO_3$ (M = Cr, Mn, Fe, Co and Ni) in air.

Compound	σ/S cm^{-1}	T/°C	Ref.
$LaCrO_3$	0.34	700	46
$La_{0.7}Sr_{0.3}CrO_3$	40	1000	47
$LaMnO_3$	80	800	48
$La_{0.7}Sr_{0.3}MnO_3$	110	700	49
$LaFeO_3$	0.1	800	50
$La_{0.7}Sr_{0.3}FeO_3$	120	700	51
$LaCoO_3$	1000	800	52
$La_{0.7}Sr_{0.3}CoO_{3-\delta}$	1650	800	53
$LaNiO_3$	40	800	50

cases, the conductivity of $La_{0.7}Sr_{0.3}MO_3$ is several orders of magnitude higher than that of unsubstituted $LaMO_3$. The alkaline-earth element should be chosen with due regard to their possible effect on the perovskite conductivity. According to the aforesaid, to reach a high conductivity, it is necessary to use large A-cations, *e.g.*, strontium (r = 1.44 Å, C.N. 12) or barium (r = 1.61 Å, C.N. 12).[45] In doing this, it should be borne in mind that the reactivity of alkaline earth metals increases in the series from calcium to barium. This means that barium-containing perovskites are most susceptible to reactions with electrolytes and also with CO_2 present in air. The latter is due to the high stability of $BaCO_3$.

3. Oxide-ion conductivity in perovskites

In contrast to the spinel structure type characteristic of many transition metal oxides (*e.g.*, Mn_3O_4, Co_3O_4, Fe_3O_4, *etc.*, which can also exhibit conductivity acceptable for cathode materials in SOFC), the perovskite structure can contain oxygen vacancies, which is important for the appearance of the oxide-ion conductivity. In the spinel structure, octahedra and tetrahedra share corners, so that the formation of oxygen vacancies is extremely disadvantageous as regards energy because should lead to anomalously low (C.N. 3) coordination of cations located in tetrahedral positions. In contrast, the formation of oxygen vacancies in the perovskite structure is possible due to the presence of stable coordination with C.N. 5 and 4 for different B-ations. One example is the Sr–Fe–O system the synthesis of which carried out under different conditions may afford either cubic perovskite $SrFeO_3$ or thermodynamically unstable $SrFeO_2$ with Fe^{2+}-cations in the square coordination.[54, 55] Besides these limiting compositions, the system contains several other phases with various oxygen stoichiometry differing in the type of ordering of oxygen vacancies.[54]

The formation of oxygen vacancies in the perovskite structure, *e.g.*, in $La^{3+}_{1-x}Sr^{2+}_x(Ga^{3+}_{1-y}Mg^{2+}_y)O_{(x+y)/2}$, is possible by the heterovalent substitution of cations with lower oxidation states for the A and/or B cations. For perovskites containing transition metal cations, an important condition for the formation of oxygen vacancies is the ability of B-cation to change its oxidation state. In this case, the heterovalent substitution of cations does not necessarily give oxygen vacancies. Thus, for $La_{1-x}Sr_xCoO_3$ perovskites synthesized in air at a low degree of substitution (x = 0.1), no significant number of oxygen vacancies is formed due to the increase in the oxidation state for some Co^{3+} cations to Co^{4+}. It should be borne in mind that cobalt in the oxidation state +4 is unstable, so that the increase in the Co^{4+} content leads to the formation of oxygen-deficient compositions $La_{1-x}Sr_xCoO_{3-\delta}$ (see Ref. 56).

The dependence of the oxide-ion conductivity on the concentration of oxygen vacancies and their mobility in the oxide lattice is expressed as

$$\sigma = ne\mu$$

where n is the concentration of oxygen vacancies, e and μ are the charge and the mobility of holes, respectively.

The oxide-ion conductivity in perovskites $ABO_{3-\delta}$ proceeds by the vacancy mechanism. Oxygen ions diffuse from occupied to vacant positions along the edge of a BO_6 octahedron (Fig. 7 *a*). When migrating from the occupied to the neighbouring vacant position, an oxygen ion moves along an arc trajectory rather than along a linear one (the shortest), as demonstrated by both computer simulation and experimental studies (analysis of high-temperature neutron diffraction data by the maximum entropy method).[57–60] During the migration, the oxygen ion passes through the saddle point which corresponds to the centre of the triangle formed by two A-cations and one B-cation (Fig. 7 *b*). The radius of the 'bottle-neck' (r') centred at the saddle point, calculated from the ion radii of cations in the perovskite structure, should be close to the oxygen ionic radius, 1.40 Å (see Ref. 45).

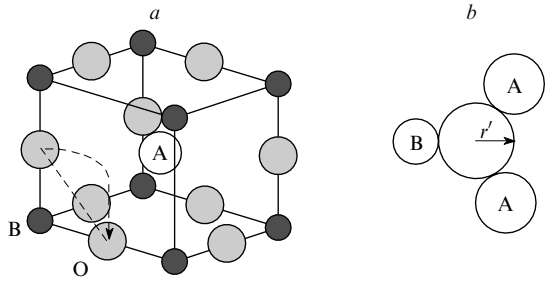


Figure 7. Schemes illustrating the mechanism of diffusion of oxygen ions in the perovskie structure.
(*a*) Oxygen ions migrated to a vacant position by the trajectory depicted by a dashed line along the edge of the BO_6 octahedron; (*b*) oxygen ion passes the saddle point with the centre at the triangle between two cations A and one cation B. The 'bottle-neck radius' (r') is determined by the ionic radii of A- and B-cations.

In the literature, a certain correlation was noted between the r' value and the oxide-ion conductivity of perovskites.[61] Indeed, the r' value for the majority of cations in the perovskite structure is much smaller than the oxygen radius ($\leqslant$1.05 Å).[62] This means that as an oxygen ion migrates through the saddle point, A- and B-cations should undergo considerable (up to $\sim$0.1 Å) shifts from their equilibrium positions.[57] There are also structural characteristics of perovskite oxides that are well correlated with the oxide-ion conductivity: the tolerance factor,[57, 61–63] the free volume (unit cell volume minus the volume of ions present in the cell), the metal–oxygen bond energy,[63] the extent of deviation of cation dimensions from 'ideal' values.[62] The last-mentioned issue means that the ionic radius of A-cation is close to the oxygen ionic radius and also that the radius of

B-cation is close to the radius of the octahedral void in this AO_3 close-packing (0.64 Å).[62] Taking into account the fact that interaction between cation B and an oxygen atom should be minimized in order to make possible the oxygen-ion conductivity, it can be concluded that as compared with $A^{II}B^{IV}O_3$, the complex perovskites with the $A^{III}B^{III}O_3$ composition should exhibit higher oxide-ion conductivity.[62, 64]

4. Crystal structure and oxide-ion conductivity in oxygen-deficient perovskites with ordered anionic vacancies

For a high concentration of oxygen vacancies, the probability exists for their ordering to form various crystal structures which can be considered as the derivatives of the perovskite structure (*e.g.*, see Ref. 65). This affects the mobility of oxygen vacancies and, hence, the oxide-ion conductivity. The realization of one or another type of ordering of oxygen vacancies often depends on the nature of A and B cations. Thus, oxides with the composition $A_2B_2O_5$ ($ABO_{2.5}\square_{0.5}$, $\square$ is the oxygen vacancy) are crystallized, most often, in the brownmillerite structural type (Fig. 8). In this structure, oxygen vacancies are ordered into layers to afford layers of corner-sharing octahedra alternating with oxygen-deficient layers comprising chains of tetrahedra.

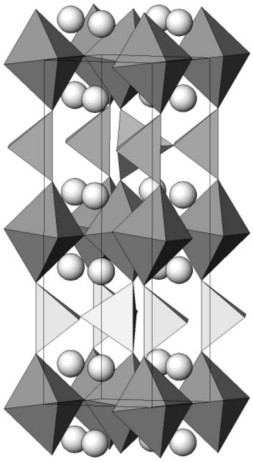


Figure 8. Crystal structure of brownmillerite $Ca_2(Fe,Al)_2O_5$.

The brownmillerite structural type embraces the oxides containing a single B-cation which is stable in both octahedral and tetrahedral coordination ($Sr_2Fe_2O_5$,[66] $Ca_2Fe_2O_5$,[67] $Ba_2In_2O_5$ [68] or $Sr_2In_2O_5$ [69]). Moreover, the brownmillerite structure turns out to be stable when the oxide composition contains two B cations prone to octahedral or tetrahedral coordination (due to geometrical factors or electronic effects). This can be exemplified by oxides containing Jahn–Teller cations Cu^{2+} ($3d^9$) or Mn^{3+} ($3d^4$), namely, $LaSrCuGaO_5$ (Ref. 70) and A_2GaMnO_5, where A = Ca, Sr.[71, 72] In $Sr(Ca)_2(Co,Ga)_2O_5$, partial ordering of cations in the brownmillerite structure is observed with octahedral coordination being preferred for Co^{3+} (Refs 73 and 74). However, under certain conditions, oxides $A_2B_2O_5$ can have a structure different from that of brownmillerite. Thus, the $A_2Mn_2O_5$ (A = Ca, Sr) and $La_2Cu_2O_5$ structures in which Mn^{3+} and Cu^{2+} cations have stable coordination with C.N. < 6 contain square pyramids BO_5 bound by all corners.[75–77] The effect of the geometric factor on the crystal structure of $A_2B_2O_5$ oxides can be clearly followed for the $SrGa_{1-x}Sc_xO_{2.5}$ system: depending on the quantitative ratio between Ga^{3+} and Sc^{3+} cations, the phases with the structure of cubic perovskite ($x = 0.25$) or brownmillerite ($x = 0.5$) can be formed or some another version of ordering of tetrahedral and octahedral cations is realized ($x = 0.4$).[78]

The effect of ordering of oxygen vacancies on their mobility in perovskite-like phases can be exemplified by the $Ba_2In_2O_5$ oxide. This oxide, which has the brownmillerite structure at room temperature, is transformed at 930 °C into a phase with the structure of cubic perovskite. The transformation is accompanied by a stepwise increase in oxide-ion conductivity by almost two orders of magnitude.[79] The cubic perovskite phase can be stabilized by the partial substitution of cations in A-sublattice. Thus the $(Ba_{0.3}Sr_{0.2}La_{0.5})_2In_2O_{5.5}$ composition demonstrated a high oxide-ion conductivity equal to 0.12 S cm^{-1} at 800 °C.[80] It deserves mention that perovskites with ordered oxygen vacancies can exhibit high oxide-ion conductivity as well. Examples are the complex oxides $RBaCo_2O_{5+\delta}$ (here, R is a REM or Y), in the crystal structure of which A-cations and oxygen vacancies are ordered (see below).

IV. Thermal expansion coefficient of oxides with the perovskite structure

The matching values of thermal expansion coefficients for the adjoining components in SOFC, for instance, the electrolyte and the cathode material, is one of the important requirements which should be taken into account when selecting materials for SOFC. Table 3 shows the TEC values for various oxides including SOFC electrolytes.

The thermal expansion coefficient of a solid is related to the asymmetry of the interatomic potential, which leads to anharmonicity of thermal displacements of atoms from their equilibrium positions. For crystalline solids, the TEC can be calculated with the use of the Morse potential in terms of the Debye model for the frequency distribution of

Table 3. Thermal expansion coefficients of various oxides in air in the temperature range of 25–900 °C.

Compound	TEC /ppm K^{-1}	Ref.
$LaMnO_3$	10.7	81
$La_{0.7}Sr_{0.3}MnO_3$	11.7	81
$LaFeO_3$	9.5	50
$La_{0.8}Sr_{0.2}Co_{0.2}Fe_{0.8}O_{3-\delta}$	15.4	82
$LaCoO_3$	21	83
$La_{0.7}Sr_{0.3}CoO_{3-\delta}$	20.8	84
$LaNiO_3$	13.2	50
$La_2NiO_{4+\delta}$	13.6	24
La_2CuO_4	12.3	30
Pr_2CuO_4	11.8	31
SOFC electrolytes		
8YSZ (see [a])	10.8	85
20GDC (see [b])	12.8	86
LSGM (2020) (see [c])	12.4	87

[a] $Zr_{0.84}Y_{0.16}O_{1.92}$; [b] $Ce_{0.8}Gd_{0.2}O_{1.9}$; [c] $La_{0.8}Sr_{0.2}Ga_{0.8}Mg_{0.2}O_{2.8}$.

the Morse oscillator.[88] This model can also be applied to calculations of TEC for perovskite-like oxides.[89,90] Besides, the TEC depends on the magnetic, electronic or ferroelectric transitions and can also change with the chemical composition as the temperature increases. The latter factor is extremely important for certain transition metal oxides including perovskites in the crystal structures of which the concentration of oxygen vacancies can increase with the increase in temperature, which is accompanied by the decrease in the oxidation state of the transition metal and, correspondingly, by the elongation of the metal–oxygen bonds. Both these factors determine the chemical expansion and have a pronounced effect on the TEC. As a result, the TEC can substantially increase at temperatures of $> 400-600$ °C in air. For example, TEC of cubic perovskite $Sr_{0.75}Y_{0.25}Fe_{0.75}Co_{0.25}O_{3-\delta}$ was observed to increase from 14.6 ppm K^{-1} in the temperature range of 100–400 °C up to 22.1 ppm K^{-1} at 400–800 °C.[91]

The electronic effects, particularly, the thermally activated transitions between different spin states of a transition metal cation also substantially affect the TEC. As seen from Table 3, the TEC of $LaCoO_3$ substantially exceeds those of $LaFeO_3$ or $LaNiO_3$. The high TEC of Co^{3+}-containing complex oxides is caused by spin transitions between the low (LS, $t_{2g}^6 e_g^0$) and high-spin (HS, $t_{2g}^4 e_g^2$) states of the cobalt(III) cation.[92] For $LaCoO_3$, the activation energy of the transition between LS and HS states of Co^{3+} is low and, depending on the temperature, varies from 20 to 80 meV.[93] At low temperatures, the Co^{3+} cation in $LaCoO_3$ is in the ground LS state, while as the temperature increases, the HS state of Co^{3+} is thermally activated. Insofar as ionic radii of Co^{3+} ions in the LS and HS states (0.525 and 0.61 Å, respectively[45]) differ by ~ 0.1 Å, the transition of a part of Co^{3+} to the HS state is accompanied by a substantial increase in the average length of the Co–O bond and in the TEC value of cobalt-containing perovskites.

The effect of the presence of Co^{3+} on the TEC can be illustrated by the example of $La_2Co(Ti_{1-x}Mg_x)O_6$ perovskites.[94] Since the crystal structure of these phases contains Ti^{4+} and Mg^{2+} cations in the octahedral coordination, the content of oxygen atoms in these phases remains unchanged in air. This makes it possible to exclude the effect of chemical expansion on the TEC. Depending on the ratio between Ti^{4+} and Mg^{2+} cations (x), the cobalt oxidation state varies from +2 ($x = 0.0$) to +3 ($x = 0.5$). As follows from Fig. 9, the TEC of $La_2Co(Ti_{1-x}Mg_x)O_6$ increases from 9 ppm K^{-1} for the composition containing exclusively Co^{2+} ($x = 0.0$) to 19 ppm K^{-1} for the case of Co^{3+} ($x = 0.5$). It should be noted that the increase in the Co^{3+} content [increase in subscript z in $La_2Co_{1+z}(Ti_{0.5}Mg_{0.5})_{1-z}O_6$] does not induce further increase in TEC.

A method for lowering down the TEC of complex oxides containing Co^{3+} cations in the octahendral coordination is to search for compounds that contain Co^{3+} cations in the ground HS state. The spin state of Co^{3+} in oxide compounds depends on the coordination surrounding. Thus, at low temperatures, the $LaCoO_3$ and $EuCoO_3$ perovskites contain Co^{3+} exclusively in the LS state.[95] In $LaSrCoO_4$, Co^{3+} cations with octahedral coordination are in the mixed (LS+HS) state even at low temperatures.[96,97] In the $Ca_3Co_2O_6$ structure, which contains Co^{3+} in the octahedral and trigonal-prismatic surrounding, the cobalt cations are in the LS state.[98] In the layered cobalt-containing oxides

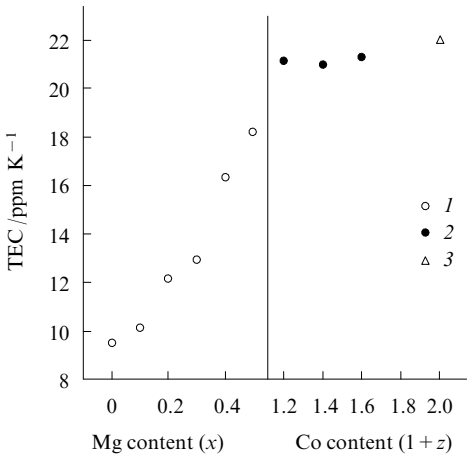


Figure 9. Thermal expansion coefficient of $La_2Co(Ti_{1-x}Mg_x)O_6$ *vs.* the content of magnesium (*1*) and TEC of $La_2Co_{1+z}(Ti_{0.5}Mg_{0.5})_{1-z}O_6$ *vs.* the content of cobalt (*2*) (point *3* corresponds to $LaCoO_3$).[91]
The composition with $x = 0.0$ corresponds to the Co^{2+} oxidation state; the composition with $x = 0.5$ corresponds to Co^{3+}. Points on the right side correspond to compositions containing only Co^{3+} ions the relative content of which increases according to the formula $La_2Co_{1+z}(Ti_{0.5}Mg_{0.5})_{1-z}O_6$.

such as Sr_2CoO_3Cl (Ref. 95) and $GdBaCo_2O_{5.5}$ (Ref. 99) with cobalt cations in the tetrahedral-pyramidal coordination, the Co^{3+} HS state is stabilized. The unique examples of the Co^{3+} stabilization in octahedral surrounding are $Sr_2Co_{2-x}Ga_xO_5$ oxides with the brownmillerite structure (see Fig. 8). The existence of the HS state for Co^{3+} in these phases was confirmed by the results of low-temperature neutron diffraction and X-ray near edge absorption spectroscopy of cobalt. The presence of Co^{3+} in the HS state in oxides with the brownmillerite structure is associated with strongly distorted octahedral coordination. In $Sr_2Co_{1.2}Ga_{0.8}O_5$, the Co–O bond lengths in the octahedron at 2 K are equal to 1.9591(4) Å for $Co-O_{eq}$ and 2.257(6) Å for $Co-O_{ax}$, whereas in $LaCoO_3$ at 5 K, the Co–O bond length is 1.925 Å and increases to 1.962 Å only at 1000 K.[100] This explains the low TEC values for cobalt-containing oxides with the brownmillerite structure (for instance, for $Sr_2Co_2O_5$, TEC = 11.75 ppm K^{-1} at 25–400 °C),[101,102] which is virtually a half of the TEC value for $LaCoO_3$ (see Table 3).

The TEC values for various oxides correlate with the concentration of oxygen vacancies in their structures. This can be illustrated by the data for perovskites for which the oxygen non-stoichiometry is determined by the degree of heterovalent substitution in the A or B sublattices, namely, for $La_{1-x}Sr_x\ Ga_{1-y}Mg_yO_{3-(x+y)/2}$ (LSGM).[103] Moreover, in many publications, the strong correlation between oxide-ion conductivity of compounds and their TEC values was noted: the compounds with high oxide-ion conductivity had also high TEC values.[104]

V. Brief summary of Sections II–IV

As regards the set of the key properties important for practical use as cathode materials in IT-SOFC, the perovskite-like oxides $ABO_{3-\delta}$ containing 3d-transition metals

B = Mn, Fe, Co, Ni and Cu proved to be most suitable. A standard cathode material for high-temperature SOFC based on lanthanum manganite doped with alkaline-earth cations (*e.g.*, LSM [105, 106]) exhibits no significant oxide-ion conductivity (see Table 1) and, hence, cannot be considered as a promising cathode material for IT-SOFC. The formation of oxygen vacancies in $LaMnO_3$ is hindered due to the great difference in ionic ra dii of Mn^{2+} and Mn^{3+} (0.82 and 0.65 Å, respectively) [45] and also due to the absence of energy benefit from reduction of Mn^{3+} ($t_{2g}^3e_g^1$) to Mn^{2+} ($t_{2g}^3e_g^2$). The partial substitution of strontium ions for lanthanum in LSM leads to the appearance of Mn^{4+} with the $3d^3$ electronic configuration which, like Cr^{3+}, exhibits high stability in the octahedral surrounding. This inhibits the formation of oxygen vacancies and diffusion of oxygen ions.

When selecting cathode materials, the cost of the oxide of a given 3d-metal should be taken into account. The cheapest are iron oxides; the commercial prices of Co, Ni, Mn and Fe oxides are related as of 10 : 6 : 2 : 1.[107] Unfortunately, the literature data on the diffusion and surface exchange coefficients of oxygen are scarce for iron-containing oxides and analysis of available data (see Table 1) makes it possible to assume a low oxide-ion conductivity in doped peroskites based on $LaFeO_3$. However, recently, information on the high efficiency of cathode materials based on perovskite-like complex iron oxides $Bi_{0.5}Sr_{0.5}FeO_{3-\delta}$ (Ref. 108) and $Sr_{0.9}K_{0.1}FeO_3$ (Refs 109 and 110) appeared. Perovskites containing cobalt and iron cations, such as $La_{1-x}Sr_xCo_{1-y}Fe_yO_{3-\delta}$ (LSCF) and $Ba_{1-x}Sr_xCo_{1-y}Fe_yO_{3-\delta}$ (BSCF), are characterized by high D^* and k values; hence, they can be considered as potential cathode materials for IT-SOFC.[111, 112] It should be noted that many iron-containing perovskites are of considerable interest as materials for ceramic membranes which are used to separate oxygen from gas mixtures; the problems of defect formation in such perovskites were discussed in detail.[113–117]

Cobalt-, nickel- and copper-containing oxides exhibit high electronic conductivity and considerable mobility of oxygen ions (see Table 1). This is why the compounds based on them can be considered as the most promising materials for IT-SOFC. Among cobalt-containing oxides, most interesting are the compounds with the Co^{3+}/Co^{4+} redox pair, for instance, $La_{1-x}Sr_xCoO_{3-\delta}$ perovskites. When going to nickel and copper compounds, one should take into account that the stability of high oxidation states of these metals lowers down as the number of d-electrons increases. For this reason, $LaNiO_3$, which contains Ni^{3+}, is unsuitable for high-temperature devices, being unstable in air at SOFC working temperatures.[118] For nickel- and copper-containing complex oxides, most promising are layered perovskite-like phases pertaining to the homologous series of Ruddlesden–Popper $A_{n+1}B_nO_{3n+1}$ (A is a REM, B = Ni, Cu, n = 1, 2, 3 is the number of BO_2 layers in the perovskite block) (Fig. 10). Examples of such oxides are $La_2NiO_{4+\delta}$, $La_3Ni_2O_{7-\delta}$, $La_4Ni_3O_{10-\delta}$, La_2CuO_4. Due to incorporation of the LaO^+ block with the rock salt structure, the oxidation state of the transition metal in these compounds is lower than +3 (*e.g.*, +2, as in La_2CuO_4), which determines the higher stability of these phases as compared with $LaMO_3$ perovskites (M = Ni, Cu). Bearing this in mind, the nickel and copper-containing complex oxides with the layered perovskite-like structure are considered as the promising cathode materials for IT-SOFC.

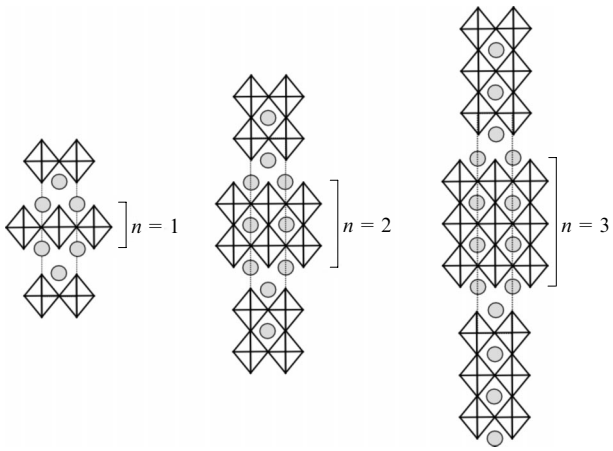


Figure 10. Schematic of crystal structures in the homologous series of the Ruddlesden–Popper phases $A_{n+1}B_nO_{3n+1}$ (n is the number of BO_2 layers in the perovskite block).

VI. Cobalt-containing perovskites

The first mention of the possibility of using $LaCoO_3$ doped with alkaline earth cations as the cathode material for SOFC dates back to the early 1980s.[119] The conductivity of $La_{1-x}Sr_xCoO_{3-\delta}$ exceeds 1000 S cm^{-1} (see Table 2) at the SOFC working temperatures, it is characterized by a high oxygen self-diffusion coefficient and high catalytic activity in the oxygen reduction process (see Table 1). As was noted above, the main drawback of cobalt-containing perovskites is their high TEC associated with transitions between the low and high-spin states of Co^{3+}. Furthermore, the cobalt-containing perovskites are extremely reactive with respect to YSZ-based electrolytes. For instance, $La_{1-x}Sr_xCoO_{3-\delta}$ reacts readily with the YSZ electrolyte to form non-conducting strontium zirconate-based phases.[120] One of the methods to reduce the reactivity towards YSZ is to deposit a protective GDC layer between the cathode material and YSZ, this layer being inert with respect to cobalt-containing oxides at the deposition temperature. However, in this case, too, the complications arise upon long-term operation of SOFC, which are associated with the diffusion of cations through the GDC layer. Another widely used method consists of the partial replacement of cobalt by another B-cation, usually a manganese, iron, nickel or copper.[32]

Perovskites $La_{1-x}Sr_xCo_{1-y}Fe_yO_{3-\delta}$ (LSCF) are the most well known and commercially promising as an alternative to LSM.[83, 121, 122] By varying the strontium and iron contents in LSCF, the $La_{0.6}Sr_{0.4}$ $Fe_{0.8}Co_{0.2}O_{3-\delta}$ composition with the optimally balanced values of TEC and high-temperature conductivity was found: TEC = 15.4 ppm K^{-1} and σ > 100 S cm^{-1} at 800 °C. Yet another widely known material based on doped cobalt-containing perovskites is $Ba_{1-x}Sr_xCo_{1-y}Fe_yO_{3-\delta}$ (BSCF).[123] Of most interest is $Ba_{0.5}Sr_{0.5}Co_{0.8}Fe_{0.2}O_{3-\delta}$ with the perovskite cubic structure. A cathode material based on this compound exhibited the lowest specific polarization resistance of the cathode/LSGM electrolyte interface, which was as low as 0.04 Ω cm^2 at 800 °C.[124] However, BSCF materials have high TEC ($\sim$ 20 ppm K^{-1}) and, moreover, they are thermodynamically unstable at high temperatures. It was shown [125, 126]

that long-term annealing in the temperature range of 700–900 °C results in transformation of the cubic BSCF into hexagonal. The presence of barium cations in the BSCF structure determines the 'vulnerability' of the latter with respect to gaseous CO_2 (Ref. 127) due to the easy formation of thermodynamically stable $BaCO_3$.

Recently, attention was focused on layered perovskite-like oxides $RBaCo_2O_{5+\delta}$ (R is an REM cation, *e.g.*, Pr or Gd). The crystal structure of these phases (Fig. 11) involves barium and REM cations ordered in layers together with ordering of oxygen vacancies. These oxides are characterized by high coefficients of diffusion and surface exchange of oxygen. Thus, for $PrBaCo_2O_{5+\delta}$ the values of D^* and k at 450 °C were found to be 4.1×10^{-9} cm^2 s^{-1} and 2.16×10^{-7} cm s^{-1} (Ref. 128) and for $GdBaCo_2O_{5+\delta}$ at 496 °C these coefficients were 2.8×10^{-10} cm^2 s^{-1} and 7.4×10^{-8} cm s^{-1} (Ref. 129), respectively. The higher diffusion coefficient of $PrBaCo_2O_{5+\delta}$ as compared with $GdBaCo_2O_{5+d}$ is caused by the larger radius of Pr^{3+} cation [$r(Pr^{3+}) = 1.126$ Å, r (Gd^{3+}) = 1.053 Å (Ref. 45)] and, hence, by larger interplanar spacing in $PrBaCo_2O_{5+\delta}$ and, as a consequence, larger free space for diffusion of oxygen ions. The specific polarization resistance of the cathode/GDC electrolyte interface for cathode materials based on $RBaCo_2O_{5+\delta}$ is 0.25 Ω cm^2 for R = Gd at 625 °C and for R = Pr at 550 °C.[129] The main drawback of $RBaCo_2O_{5+\delta}$ is the high TEC value which, depending on the nature of REM cation, varies from 16 to 24 ppm K^{-1} (Refs 130 and 131). Furthermore, due to the presence of a barium cation in $RBaCo_2O_{5+\delta}$, these oxides are sensitive with respect to the CO_2 present in the gas phase.

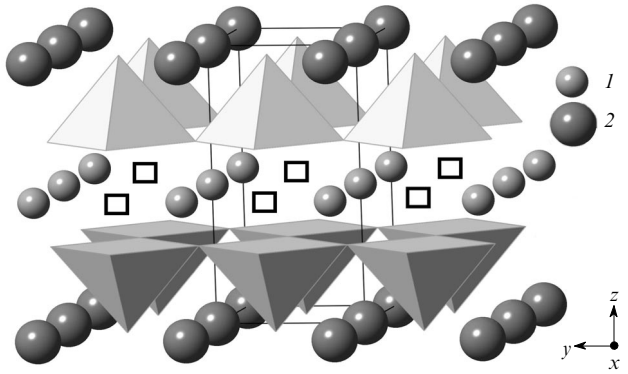


Figure 11. Crystal structure of $RBaCo_2O_{5+\delta}$.
The oxygen vacancies designated by squares can be partially populated by oxygen ions, depending on the size of the REM cation. (*1*) R, (*2*) Ba.

Other actively explored cobalt-containing oxides are $Sr_{0.75}R_{0.25}CoO_{2.62}$ (R = REM and Y) with the structure of the so-called 314-phases (Fig. 12 *a*).[132, 133] As for $RBaCo_2O_{5+\delta}$, the crystal structure of 314-phases demonstrates the ordering of A-cations and oxygen vacancies. The structure of 314-phases contains oxygen-deficient layers separated by layers of corner-sharing CoO_6 octahedra. The oxygen-deficient layers (Fig. 12 *b*) are built of four CoO_4 tetrahedra connected into rings. The additional oxygen atoms supplement the coordination number of some cobalt cations to 5. As a result, the 'ideal' structure of 314-phases corresponding to the composition $Sr_{0.75}R_{0.25}CoO_{2.625}$

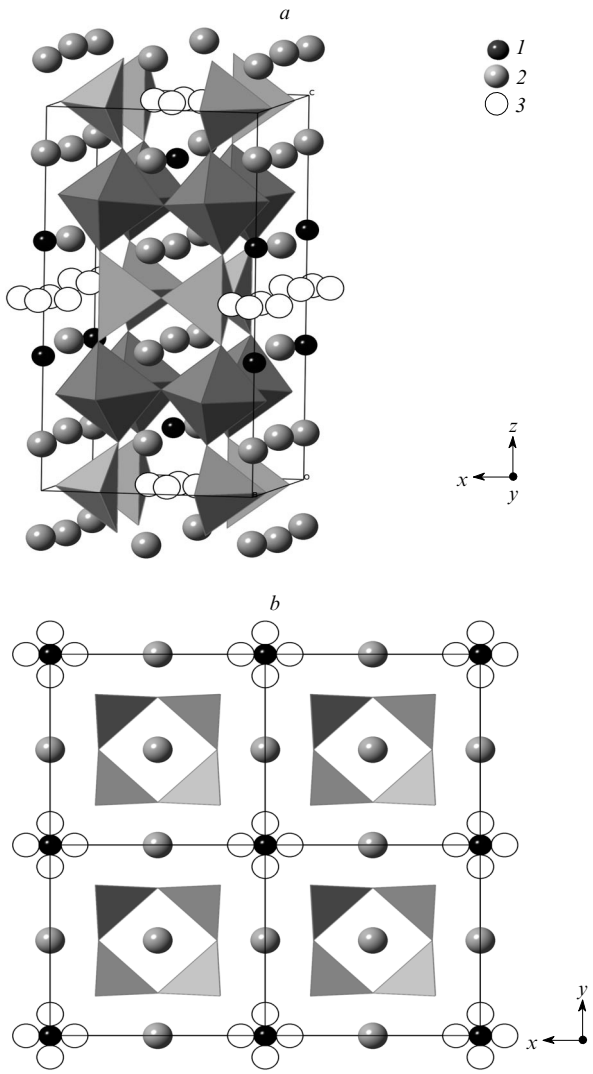


Figure 12. Crystal structure of 314-phases ($Sr_{0.75}R_{0.25}CoO_{2.62}$, R = REM and Y) (*a*) and projection of the structure of the oxygen-deficient layer (4 unit cells are shown) (*b*).
(*1*) R-cations, (*2*) Sr cations, (*3*) additional oxygen atoms in the oxygen-deficient layer. The position of additional oxygen atoms is populated by 1/4.

includes an oxygen-deficient layer built of equal numbers of cobalt cations with C.N. 4 and C.N. 5. Calculations of the migration routes of oxygen ions in $Sr_{0.75}Y_{0.25}CoO_{2.625}$, which were carried out by molecular dynamics methods, have shown that the oxide-ion conductivity is isotropic.[134] The calculated values of activation energy of diffusion of oxygen ions were confirmed experimentally.[28] Coefficients D^* and k for $Sr_{0.75}Y_{0.25}CoO_{2.625}$ are comparable with those of LSCF (see Table 1) and the specific resistance of the cathode/GDC electrolyte interface is 0.09 Ω cm^2 (770 °C). Model SOFC with cathodes made of $Sr_{0.7}Y_{0.3}CoO_{2.625}$ and $Sr_{0.7}Ho_{0.3}CoO_{2.625}$ and the LSGM electrolyte has demonstrated[135, 136] their high power densities, which reached 0.93 W cm^{-2} at 850 °C for $Sr_{0.7}Y_{0.3}CoO_{2.625}$ and 1.27 W cm^{-2} at 850 °C for $Sr_{0.7}Ho_{0.3}CoO_{2.625}$.

However, like the majority of Co^{3+}-containing perovskites, $Sr_{0.75}Y_{0.25}CoO_{2.625}$ demonstrates a high TEC, which reaches 20 ppm K^{-1} (Ref. 92). This is associated with the

fact that Co^{3+}, which has the octahedral surrounding in this phase, occurs in the mixed (LS + HS) state. This suggests that the magnetic moment of Co^{3+} cations is $\sim 1.2\ \mu_B$ (at 14 K), which was confirmed by the neutron diffraction data.[137] To reduce the TEC, some cobalt ions were replaced by manganese, iron and nickel cations.[92, 138–140] The optimal characteristics were observed for $Sr_{0.75}Y_{0.25}Co_{0.5}Mn_{0.5}O_{3-\delta}$, namely, TEC = 15.5 ppm K^{-1}, the conductivity of 110 S cm^{-1} in air at 900 °C.[138, 139] The power density of a model SOFC containing this cathode material and an YSZ-based electrolyte with the GDC layer was found to be higher as compared with the case of LSM.[139, 140]

VII. Nickel and copper-containing complex oxides with layered structures

Recently, the interest was heightened in nickel and copper-containing oxides $R_2MO_{4+\delta}$ (M = Ni, Cu) with the layered perovskite-like structure as the promising materials for IT-SOFC. Depending on the nature of cations, these oxides are crystallized in the K_2NiF_4 structural type, the so-called T- (see Figs 10 and 13 *a*), T′- (Fig. 13 *b*) and T*-phases (see Fig. 13 *c*). The first version is realized for $R_2NiO_{4+\delta}$ and La_2CuO_4, the second is realized for R_2CuO_4 with other rare-earth cations up to Gd_2CuO_4. The arrangements of a part of atoms in these structures is similar, *i.e.*, both contain similar layers of CuO_2 and R cations. However, the positions of the rest of oxygen atoms considerably differ. In the T-phase structure, oxygen atoms totally occupy all octahedral positions in the R_2O_2 block, whereas tetrahedral voids are either unoccupied (La_2CuO_4) or partly occupied ($R_2NiO_{4+\delta}$). In the T′-phase structure, the octahedral voids remain vacant and tetrahedral voids are populated by oxygen atoms. This results in different coordination of cations R and M, *i.e.*, the coordination number of cation M is 6 (octahedron) in the T-phase and 4 (square) in the T′-phase, whereas for cation R, the C.N. is 9 (T-phase) and 8 (T′-phase). In other words, the crystal structure of $R_2MO_{4+\delta}$ (M = Ni, Cu) oxides is often considered as intergrowth structure between the perovskite blocks and blocks with the rock salt (T-phase) or fluorite (T′-phase) structure. When two different-sized A-cations are present in a complex copper oxide, the T*-phase can be formed. In the latter case, the structure contains equal number of blocks with the rock-salt and fluorite structures (see Fig. 13 *c*), so that the transition metal C.N. becomes equal to 5 (tetragonal pyramid).

A peculiarity of these crystal structures is the presence of vacant anionic positions in rock-salt blocks along which the diffusion of oxygen ions can proceed. For T-phases, these positions can be partly occupied and the composition of nickel-containing oxides (but not La_2CuO_4) can be written as $R_2NiO_{4+\delta}$. The number of additional oxygen atoms (δ) depends on the nature of REM cation: $\delta = 0.16$ for R = La and $\delta = 0.21-0.23$ for R = Nd and Pr (δ values correspond to samples prepared by slow cooling in air from 900 °C).[141, 142] It deserves mention that the crystal structures of $R_2NiO_{4+\delta}$ are distorted as compare d with the ideal T-phase structure with the tetragonal lattice (space group $I4/mmm$).

Due to mismatch between the Ni–O and R–O distances in the $R_2NiO_{4+\delta}$ crystal structures, the rotation of NiO_6 octahedra occurs, which lowers down the symmetry to orthorhombic [$a_{ortho} \approx b_{ortho} \approx \sqrt{2}\,a_{tetr}$, $c_{ortho} \approx c_{tetr}$, space group *Fmmm* (R = La) or *Bmab* (R = Pr, Nd)].[141] The degree of orthorhombic distortion of the structure increases with the decrease in the radius of the REM cation. It is assumed that the number of additional oxygen atoms in the crystal structure of nickel-containing phases correlates with the degree of distortion of the crystal structure, which is associated with the necessity of removal of structural strains that arise due to the decrease in the ionic radius of REM on going from La to Pr and Nd.[143]

The oxides R_2NiO_{4+d} are characterized by high coefficients D^* and k (see Table 1). Studying the diffusion of

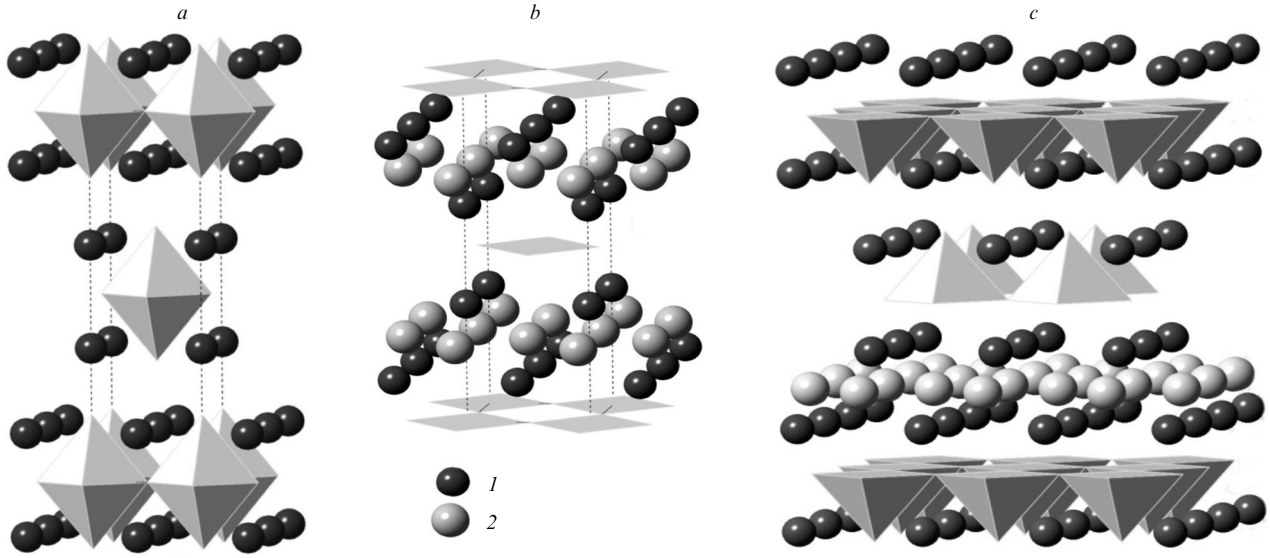


Figure 13. Crystal structure of the T-phase $R_2NiO_{4+\delta}$ and La_2CuO_4 (*a*), T′-phase R_2CuO_4 (R = Pr–Gd) (*b*) and T*-phase (*c*). (*1*) R-cations, (*2*) oxygen ions.

oxygen ions in these oxides by molecular dynamics methods has shown [144] that the oxygen transport proceeds by the interstitial mechanism in the block with the rock salt structure. Oxygen ions in axial positions of NiO_6 octahedra also take part in this process.

At the temperature < 800 °C, the $Pr_2NiO_{4+\delta}$ oxide has the oxygen diffusion coefficient higher than $R_2NiO_{4+\delta}$ (R = La, Nd) and its conductivity exceeds 100 S cm^{-1} in a wide temperature range.[141] The thermal expansion coefficient of $R_2NiO_{4+\delta}$ is close to the TEC of the GDC electrolyte (see Table 3), and the phase transitions that occur in the temperature ranges of 423–473 K ($La_2NiO_{4+\delta}$), 823–873 K ($Nd_2NiO_{4+\delta}$) [141] and also at 720 K ($Pr_2NiO_{4+\delta}$) [145] are not accompanied by changes in the volume and, hence, create no problems during the operation of a SOFC with the cathode based on these oxides. A comparative study of $R_2NiO_{4+\delta}$ in symmetric cells with the electrolyte based on YSZ and a buffer layer based on doped CeO_2 has shown [146] that the lowest specific polarization resistance of the cathode/electrolyte interface is exhibited by $Pr_2NiO_{4+\delta}$. Furthermore, studying the model SOFC of the anode-supported design, with YSZ-based electrolyte and cathode materials based on $Pr_2NiO_{4+\delta}$ at 600 °C has shown that under similar experimental conditions, the cathode material surpasses LSCF. For model SOFC with cathode materials based on $La_{2-x}Pr_xNiO_{4+\delta}$, it was found that $Pr_2NiO_{4+\delta}$ exhibits the highest efficiency.[147] Wan *et al.*[148] have prepared $Nd_{2-x}La_xNiO_{4+\delta}$ cathode materials and studied model SOFC with electrolytes based on GDC and LSGM. Of GDC-based electrolytes, $Nd_2NiO_{4+\delta}$ had the best characteristics; among LSGM electrolytes, the best was $Nd_{0.8}La_{1.2}NiO_{4+\delta}$.

A study of chemical reactions between the electrolyte and $R_2NiO_{4+\delta}$ has shown that $Pr_2NiO_{4+\delta}$ is oxidized at temperature of > 850 °C to form $Pr_4Ni_3O_{10}$ and Pr_6O_{11} (Refs 149–151). The oxide $La_2NiO_{4+\delta}$ reacts with GDC and YSZ at 700 and 900 °C, respectively, whereas $Nd_2NiO_{4+\delta}$ does not react with these electrolytes at temperatures of < 900 °C; however, at 1000 °C, the reaction does occur rather actively.

It was mentioned above that among copper-containing R_2CuO_4 oxides, only La_2CuO_4 has the T-phase structure, while the other have the T′-phase structure. According to Table 1, even at 700 °C, La_2CuO_4 demonstrates the high coefficients D^* and k and the TEC (12.3 ppm K^{-1}) close to that of the GDC electrolyte but exhibits low and virtually temperature-independent conductivity (~15 S cm^{-1} at 1000 °C [30, 152]). The cuprates R_2CuO_4 of heavier REM (R = Pr, Nd, Sm) with the semiconductor type of conduction are characterized by higher conductivity at higher temperatures [152] and their forbidden bands narrow down as the REM radius increases (the maximum conductivity of Pr_2CuO_4 was observed at 900 °C in air: >100 S cm^{-1}).[153] The thermal expansion coefficients of cuprates with the T′-phase structure are low: 11.8 ppm K^{-1} for Pr_2CuO_4 and 12.6 ppm K^{-1} for Nd_2CuO_4 and Sm_2CuO_4 (Ref. 31). According to a study of the diffusion of oxygen ions in Pr_2CuO_4, the coefficients D^* and k of Pr_2CuO_4 are considerably lower than those with La_2CuO_4 (see Table 1). This is associated with the peculiarities of the T′-phase crystal structure. Calculations of possible routes for diffusion of oxygen ions in Pr_2CuO_4 carried out by the molecular dynamic method [154] have shown that the transport of oxygen ions in the T′-phase proceeds by the interstitial mechanism and involves vacant octahedral positions in the fluorite block. From the analysis of the Pr_2CuO_4 crystal structure, it follows that the fluorite block Pr_2O_2 is compressed, so that the distance between Cu^{2+} cations and vacant octahedral positions becomes only 1.81 Å, *i.e.*, it is substantially smaller than the normal $Cu^{2+}-O$ distance. This complicates the migration of oxygen ions in the T′-phase as compared with the T-phase.

The importance of the presence of rock salt blocks in the crystal structure of layered perovskite-like oxides for the appearance of high oxide-ion conductivity has been demonstrated for $Pr_{1.6}Sr_{0.4}CuO_{3.98}$ with the T*-phase structure containing equal numbers of rocksalt and fluorite blocks (see Fig. 13 *c*). It was found that for $Pr_{1.6}Sr_{0.4}CuO_{3.98}$ the oxygen diffusion coefficient equal to 6.7 10^{-10} cm^2 s^{-1} at 700 °C is intermediate between its values for Pr_2CuO_4 and La_2CuO_4 (see Table 1).

Study of the mechanism of oxygen reduction on the Pr_2CuO_4 cathode deposited on the GDC electrolyte has shown that the process involves the three-phase boundary. Thus, the behaviour of the Pr_2CuO_4-based cathode material is similar to that of LSM.[155] For model SOFC with GDC-based electrolytes and cathodes based on the cuprates R_2CuO_4 (R = La, Nd and Pr), it was shown [156] that SOFC with Pr_2CuO_4 have the highest characteristics, namely, 100 mW cm^{-2} at 800 °C and 250 mW cm^{-2} at 900 °C. In the literature, the inertness of Pr_2CuO_4 with respect to the GDC-based electrolyte up to high temperatures was noted.[155, 156] Thus, taking into account the high conductivity and the low thermal expansion coefficient of Pr_2CuO_4, the ease of its synthesis as a single phase and also its relatively low cost, it can be concluded that this complex oxide is the cathode material of choice for IT-SOFC.

VIII. Conclusion

Oxygen-deficient perovskite-like oxides $ABO_{3-\delta}$ that contain transition metal cations hold most promise as cathode materials in IT-SOFC. This is associated with the fact that the perovskite crystal structure is capable of providing high electronic and oxide-ion conductivity. Furthermore, due to the presence of two types of cations differing as regards their crystal-chemical properties, one can tailor the properties of perovskite-like phases by substituting cations in A and/or B sublattices. Among various perovskites, the oxides containing cations of the end of the 3d-element row, namely, cobalt, nickel or copper, are the most suitable as the cathode materials.

Perovskite-like cobalt-containing oxides combine the high electrocatalytic activity in oxygen reduction with the record-breaking values of electronic and oxide-ion conductivity but have TEC far exceeding the TEC of standard SOFC electrolytes. This drawback is associated with the temperature-activated transitions between the spin states of Co^{3+} cations and can be overcome by partial substitution of other transition metal cations for cobalt cations. Another method of solving this problem is the crystal-chemical design of oxides with structural blocks, which would provide the Co–O bond length suitable for Co^{3+} stabilization in the high-spin state.

Among nickel and copper-containing complex oxides, the required stability for operation in IT-SOFC can be achieved with layered $R_2MO_{4+\delta}$ phases (R = REM and Y, M = Ni, Cu). The latter can serve as examples of bifunc-

tional materials because their crystal structure contains perovskite blocks capable of providing high electronic conductivity and also R_2O_2 blocks (with anionic vacancies), which ensure high oxide-ion conductivity. By varying the cationic composition and the structure of the R_2O_2 block in $R_2MO_{4+\delta}$, it is possible to deliberately change the important properties of the SOFC cathode material such as its electronic and oxide-ion conductivity.

We are grateful to O A Petrii, G N Mazo and S M Kazakov for their helpful comments during the work on this review. The study was performed within the framework of the Programme of Development of Moscow State University up to 2020 and was financially supported by the Ministry of Education and Science of the Russian Federation (State contract 02.740.11.0185) and by the Russian Foundation of Basic Research (Project No. 11-03-01225).

References

1. J C Larminie, A Dicks *Fuel Cell Systems Explained* (New York: Wiley, 2003)
2. E Justi, A Winsel *Kalte Verbrennung — Fuel Cells* (Wiesbaden: Franz Steiner Verlag, 1962)
3. V S Bagotskii, A M Skundin *Khimicheskie Istochniki Toka* (Chemical Cells Current Sources) (Moscow: Energoizdat, 1981)
4. B C H Steele, A Heinzel *Nature (London)* **414** 345 (2001)
5. S M Haile *Acta Mater.* **51** 5981 (2003)
6. A B Yaroslavtsev, Yu A Dobrovolsky, L A Frolova, E V Gerasimova, E A Sanginov, N S Shaglaeva *Russ. Chem. Rev.* **81** 191 (2012)
7. S S Ivanchev, S V Myakin *Russ. Chem. Rev.* **79** 101 (2010)]
8. A L Rusanov, E G Bulycheva, M G Bugaenko, V Yu Voytekunas, M J Abadie *Russ. Chem. Rev.* **78** 53 (2009)
9. S C Singhal, K Kendall, in *High Temperature Solid Oxide Fuel Cells: Fundamentals, Design and Applications* (Eds S C Singhal, K Kendall) (Oxford: Elsevier, 2003) p. 1
10. H U Anderson, F Tietz, in *High Temperature Solid Oxide Fuel Cells: Fundamentals, Design and Applications* (Eds S C Singhal, K Kendall) (Oxford: Elsevier, 2003) p. 173
11. N Q Minh *J. Am. Ceram. Soc.* **76** 563 (1993)
12. H Yokokawa, N Sakai, T Kawada, M Dokiya *J. Electrochem. Soc.* **138** 1018 (1991)
13. B C H Steele *J. Mater. Sci.* **36** 1053 (2001)
14. E Ivers-Tiffée, A V Virkar, in *High Temperature Solid Oxide Fuel Cells: Fundamentals, Design and Applications* (Eds S C Singhal, K Kendall) (Oxford: Elsevier, 2003) p. 229
15. A J Jacobson *Chem. Mater.* **22** 660 (2010)
16. A Aguadero, L Fawcett, S Taub, R Woolley, K-T Wu, N Xu, J A Kilner, S J Skinner *J. Mater. Sci.* **47** 3925 (2012)
17. J Molenda, K Swierczek, W Zajac *J. Power Sources* **173** 657 (2007)
18. D Brett, A Atkinson, N P Brandon, S J Skinner *Chem. Soc. Rev.* **37** 1568 (2008)
19. A Tarancon *Energies* **2** 1130 (2009)
20. A Orera, P R Slater *Chem. Mater.* **22** 675 (2010)
21. A Tarancon, M Burriel, J Santiso, S J Skinner, J Kilner *J. Mater. Chem.* **20** 3799 (2010)
22. E V Tsipis, V V Kharton *J. Solid State Electrochem.* **12** 1367 (2008)
23. E V Tsipis, V V Kharton *J. Solid State Electrochem.* **12** 1039 (2008)
24. E V Tsipis, V V Kharton *J. Solid State Electrochem.* **15** 1007 (2011)
25. S B Adler, J A Lane, B C H Steele *J. Electrochem. Soc.* **143** 3554 (1996)
26. A Carter, A Selcuk, R J Chater, J Kajda, J A Kilner, B C H Steele *Solid State Ionics* **53–56** 597 (1992)
27. T Ishigaki, S Yamauchi, K Kishio, J Mizusaki, K Fueki *J. Solid State Chem.* **73** 179 (1988)
28. D P Rupasov, A V Berenov, J A Kilner, S Ya Istomin, E V Antipov *Solid State Ionics* **197** 18 (2011)
29. S J Skinner, J A Kilner *Solid State Ionics* **135** 709 (2000)
30. E Boehm, J-M Bassat, M C Steil, P Dordor, F Mauvy, J-C Grenier *Solid State Sci.* **5** 973 (2003)
31. M S Kaluzhskikh, S M Kazakov, G N Mazo, S Ya Istomin, E V Antipov, A A Gippius, Yu Fedotov, S I Bredikhin, Y Liu, G Svensson, Z Shen *J. Solid State Chem.* **184** 698 (2011)
32. *Perovskite Oxide for Solid Oxide Fuel Cells* (Ed. T Ishihara) (New York: Springer, 2009)
33. J Kilner, S J Skinner, H H Brongersma *J. Solid State Electrochem.* **15** 861 (2011)
34. B C H Steele *Solid State Ionics* **134** 3 (2000)
35. A Wells *Structural Inorganic Chemistry* (Oxford: Clarendon Press, 1984)
36. R H Mitchell *Perovskites Modern and Ancient* (Thunder Bay, Ontario: Almaz Press, 2002)
37. J A M Van Roosmalen, E H P Cordfunke, R B Helmholdt, H W Zandbergen *J. Solid State Chem.* **110** 100 (1994)
38. V M Goldschmidt *Naturwissenschaften* **14** 477 (1926)
39. A M Glazer *Acta Crystallogr., Sect. B* **28** 3384 (1972)
40. K S Aleksandrov *Kristallografiya* **21** 249 (1976) [a]
41. P M Woodward *Acta Crystallogr., Sect. B* **53** 32 (1997)
42. C J Howard, H T Stokes *Acta Crystallogr., Sect. B* **54** 782 (1998)
43. J B Goodenough, in *Progress in Solid State Chemistry* Vol. 5 (Ed. H Reiss) (Oxford: Pergamon Press, 1971) p. 145
44. J B Torrance, P Lacorre, A I Nazzal, E J Ansaldo, Ch Niedermayer *Phys. Rev. B: Condens. Matter* **45** 8209 (1992)
45. R D Shannon *Acta Crystallogr., Sect. A* **32** 751 (1976)
46. V V Kharton, A A Yaremchenko, E N Naumovich *J. Solid State Electrochem.* **3** 303 (1999)
47. J W Fergus *Solid Sate Ionics* **171** 1 (2004)
48. Q He, X Zhang, H Hao, X Hu *Physica B* **403** 2867 (2008)
49. Y Sakaki, Y Takeda, A Kato, N Imanashi, O Yamamoto, M Hattori, M Iio, Y Esaki *Solid State Ionics* **118** 187 (1999)
50. R Chiba, F Yoshimura, Y Sakurai *Solid State Ionics* **124** 281 (1999)
51. K Iwasaki, T Ito, M Yoshio, T Matsui, T Nagasaki, Y Arita *J. Alloys Compd.* **430** 297 (2007)
52. J Mizusaki, M Yoshiro, S Yamauchi, K Fueki *J. Electrochem. Soc.* **136** 2082 (1989)
53. K Kakinuma, T Arisaka, H Yamamura *J. Ceram. Soc. Jpn.* **112** 342 (2004)
54. J P Hodges, S Short, J D Jorgensen, X Xiong, B Dabrowski, S M Mini, C W Kimball *J. Solid State Chem.* **151** 190 (2000)
55. Y Tsujimoto, C Tassel, N Hayashi, T Watanabe, H Kageyama, K Yoshimura, M Takano, M Ceretti, C Ritter, W Paulus *Nature (London)* **450** 1062 (2007)
56. J E Sunstrom IV, K V Ramanujachary, M Greenblatt, M Croft *J. Solid State Chem.* **139** 388 (1998)
57. M Cherry, M S Islam, C R A Catlow *J. Solid State Chem.* **118** 125 (1995)
58. M S Islam *Solid State Ionics* **154–155** 75 (2002)
59. M Yashima, K Nomura, H Kageyama, Y Miyazaki, N Chitose, K Adachi *Chem. Phys. Lett.* **380** 391 (2003)
60. T Tsuji *J. Appl. Crystallogr.* **40** 1166 (2007)
61. R L Cook, A F Sammells *Solid State Ionics* **45** 311 (1991)
62. M Mogensen, D Lybye, N Bonanos, P V Hendriksen, F W Poulsen *Solid State Ionics* **174** 279 (2004)
63. A F Sammells, R L Cook, J H White, J J Osborne, R C MacDuff *Solid State Ionics* **52** 111 (1992)
64. H Hayashi, H Inaba, M Matsuyama, N G Lan, M Dokiya, H Tagawa *Solid State Ionics* **122** 1 (1999)

65. E V Antipov, A M Abakumov, S Ya Istomin *Inorg. Chem.* **47** 8543 (2008)
66. C Greaves, A J Jacobson, B C Tofield, B E F Fender *Acta Crystallogr., Sect. B* **31** 641 (1975)
67. F Bertaut, P Blum, A Sagnieres *C. R. Acad. Sci.* **244** 2944 (1957)
68. D H Gregory, M T Weller *J. Solid State Chem.* **107** 134 (1993)
69. R von Schenk, H Müller-Buschbaum *Z. Anorg. Allg. Chem.* **395** 280 (1973)
70. J T Vaughey, J B Wiley, K R Poeppelmeier *Z. Anorg. Allg. Chem.* **598** 327 (1991)
71. A M Abakumov, M G Rozova, B P Pavlyuk, M V Lobanov, E V Antipov, O I Lebedev, G van Tendeloo, O L Ignatchik, E A Ovtchenkov, Yu A Koksharov, A N Vasil'ev *J. Solid State Chem.* **160** 353 (2001)
72. A M Abakumov, M G Rozova, B P Pavlyuk, M V Lobanov, E V Antipov, O I Lebedev, G van Tendeloo, D V Sheptyakov, A M Balagurov, F Bouree *J. Solid State Chem.* **158** 100 (2001)
73. F Lindberg, S Ya Istomin, P Berastegui, G Svensson, S M Kazakov, E V Antipov *J. Solid State Chem.* **173** 395 (2003)
74. S Ya Istomin, S V Abdyusheva, G Svensson, E V Antipov *J. Solid State Chem.* **177** 4251 (2004)
75. K R Poeppelmeier, M E Leonowicz, J C Scanlon, J M Longo, W B Yelon *J. Solid State Chem.* **45** 71 (1982)
76. V Caignaert, N Nguyen, M Hervieu, B Raveau *Mater. Res. Bull.* **20** 479 (1985)
77. N R Khasanova, F Izumi, Z Hiroi, M Takano, Q Huang, A Santoro *Acta Crystallogr., Sect. C* **52** 2381 (1996)
78. S V Chernov, Yu A Dobrovolsky, S Ya Istomin, E V Antipov, J Grins, G Svensson, N V Tarakina, A M Abakumov, G van Tendeloo, S G Eriksson, S M H Rahman *Inorg. Chem.* **51** 1094 (2012)
79. J Goodenough, J Ruez-Diaz, Y Zhen *Solid State Ionics* **44** 21 (1990)
80. K Kakinuma, H Yamamura, H Haneda, T Atake *Solid State Ionics* **154 – 155** 571 (2002)
81. A Hammouche, E Siebert, A Hammou *Mater. Res. Bull.* **24** 367 (1989)
82. L-W Tai, M M Nasrallah, H U Anderson, D M Sparlin, S R Sehlin *Solid State Ionics* **76** 259 (1995)
83. F M Figueiredo, J R Frade, F M B Marques *Solid State Ionics* **118** 81 (1999)
84. Y Ohno, S Nagata, H Sato *Solid State Ionics* **9 – 10** 1001 (1983)
85. G Stochniol, A Gupta, A Naoumidis, D Stoever, in *Proceedings of the 5th International Symposium on Solid Oxide Fuel Cells (SOFC-V)* (Eds U Stimming, S C Singhal, H Tagawa, W Lehnert) (Pennington, NJ: Electrochemical Society, 1997) p. 888
86. F Tietz *Ionics* **5** 129 (1999)
87. J W Stevenson, T R Armstrong, L R Pederson, J Li, C A Levinsohn, S Baskaran *Solid State Ionics* **113 – 115** 571 (1998)
88. A R Ruffa *J. Mater. Sci.* **15** 2258 (1980)
89. R E Williford, T R Armstrong, J D Gale *J. Solid State Chem.* **149** 320 (2000)
90. H Inaba, H Tagawa *J. Ceram. Soc. Jpn.* **106** 272 (1998)
91. S Ya Istomin, O A Drozhzhin, Ph S Napolsky, S N Putilin, A A Gippius, E V Antipov *Solid State Ionics* **179** 1054 (2008)
92. S Uhlenbruck, F Tietz *Mater. Sci. Eng., B* **107** 277 (2004)
93. M W Haverkort, Z Hu, J C Cezar, T Burnus, H Hartmann, M Reuther, C Zobel, T Lorenz, A Tanaka, N B Brookes, H H Hsieh, H-J Lin, C T Chen, L H Tjeng *Phys. Rev. Lett.* **97** 176405 (2006)
94. S Shafeie, J Grins, S Ya Istomin, A A Gippius, L Karvonen, S Populoh, A Weidenkaff, J Koehler, G Svensson *J. Mater. Chem.* **22** 16269 (2012)
95. Z Hu, H Wu, M W Haverkort, H H Hsieh, H-J Lin, T Lorenz, J Baier, A Reichl, I Bonn, C Felser, A Tanaka, C T Chen, L H Tjeng *Phys. Rev. Lett.* **92** 207402 (2004)
96. J Wang, W Zhang, D Y Xing *Phys. Rev. B: Condens. Matter* **62** 14140 (2000)
97. H Wu *Phys. Rev. B: Condens. Matter* **81** 115127 (2010)
98. T Burnus, Z Hu, M W Haverkort, J C Cezar, D Flahaut, V Hardy, A Maignan, N B Brookes, A Tanaka, H H Hsieh, H-J Lin, C T Chen, L H Tjeng *Phys. Rev. B: Condens. Matter* **74** 245111 (2006)
99. M García-Fernández, V Scagnoli, U Staub, A M Mulders, M Janousch, Y Bodenthin, D Meister, B D Patterson, A Mirone, Y Tanaka, T Nakamura, S Grenier, Y Huang, K Conder *Phys. Rev. B: Condens. Matter* **78** 054424 (2008)
100. P G Radaelli, S-W Cheong *Phys. Rev. B: Condens. Matter* **66** 094408 (2002)
101. A Muñoz, C de la Calle, J A Alonso, P M Botta, V Pardo, D Baldomir, J Rivas *Phys. Rev. B: Condens. Matter* **78** 054404 (2008)
102. C de la Calle, A Aguadero, J A Alonso, M T Fernandez-Díaz *Solid State Sci.* **10** 1924 (2008)
103. H Hayashi, M Suzuki, H Inaba *Solid State Ionics* **128** 131 (2000)
104. H Ullmann, N Trofimenko, F Tietz, D Stoever, A Ahmad-Khanlou *Solid State Ionics* **138** 79 (2000)
105. S P Jiang *J. Mater. Sci.* **43** 6799 (2008)
106. M Chen, Y-L Liu, A Hagen, P V Hendriksen, F W Poulsen *Fuel Cells* **9** 833 (2009)
107. Sh Hou, J A Alonso, Sh Rajasekhara, M J Martinez-Lope, M T Fernandez-Diaz, J B Goodenough *Chem. Mater.* **22** 1071 (2010)
108. Y Niu, W Zhou, J Sunarso, L Ge, Zh Zhu, Z Shao *J. Mater. Chem.* **20** 9619 (2010)
109. Sh Hou, J A Alonso, J B Goodenough *J. Power Sources* **195** 280 (2010)
110. Sh Hou, A Aguadero, J A Alonso, J B Goodenough *J. Power Sources* **196** 5478 (2011)
111. S J Benson, R J Chater, J A Kilner, in *Proceedings of the Second International Symposium on Ionic and Mixed Conducting Ceramics* (Pennington, NJ: Electrochemical Society, 1994) p. 9
112. L Wang, R Merkle, J Maier, T Acartürk, U Starke *Appl. Phys. Lett.* **94** 071908 (2009)
113. M V Patrakeev, J A Bahteeva, E B Mitberg, I A Leonidov, V L Kozhevnikov, K R Poeppelmeier *J. Solid State Chem.* **172** 219 (2003)
114. M V Patrakeev, E B Mitberg, A A Lakhtin, I A Leonidov, V L Kozhevnikov, V V Kharton, M Avdeev, F M B Marques *J. Solid State Chem.* **167** 203 (2002)
115. M V Patrakeev, I A Leonidov, V L Kozhevnikov, V V Kharton *Solid State Sci.* **6** 907 (2004)
116. V V Kharton, A A Yaremchenko, A P Viskup, M V Patrakeev, I A Leonidov, V L Kozhevnikov, F M Figueiredo, A L Shaulo, E N Naumovich, F M B Marques *J. Electrochem. Soc.* **149** E125 (2002)
117. E V Tsipis, M V Patrakeev, V V Kharton, A A Yaremchenko, G C Mather, A L Shaula, I A Leonidov, V L Kozhevnikov, J R Frade *Solid State Sci.* **7** 355 (2005)
118. J Takahashi, T Toyoda, T Ito, M Takatsu *J. Mater. Sci.* **25** 1557 (1990)
119. Y Ohno, S Nagata, H Sato *Solid State Ionics* **3 – 4** 439 (1981)
120. O Yamamoto, Y Takeda, R Kanno, M Noda *Solid State Ionics* **22** 241 (1987)
121. L W Tai, M M Nasrallah, H U Anderson, D M Sparlin, S R Sehlin *Solid State Ionics* **76** 273 (1995)
122. L W Tai, M M Nasrallah, H U Anderson, D M Sparlin *J. Solid State Chem.* **118** 117 (1995)
123. E Magnone *J. Fuel Cell Sci. Technol.* **7** 064001 (2010)

124. J Pena-Martinez, D Marrero-Lopez, D Perez-Coll, J C Ruiz-Morales, P Nunez *Electrochim. Acta* **52** 2950 (2007)
125. S Šarcová, K Wiik, J Tolchard, H J M Bouwmeester, T Grande *Solid State Ionics* **178** 1787 (2008)
126. Z Yang, J Martynczuk, K Efimov, A S Harvey, A Infortuna, P Kocher, L J Gauckler *Chem. Mater.* **23** 3169 (2011)
127. A Yan, M Cheng, Y Dong, W Yang, V Maragou, Sh Song, P Tsiakaras *Appl. Catal., B* **66** 64 (2006)
128. R Frison, S Poltier, M Martin, K Conder *Nucl. Instrum. Methods Phys. Res., Sect. B* **273** 142 (2012)
129. A Tarancón, S J Skinner, R J Chater, F Hernández-Ramírez, J A Kilner *J. Mater. Chem.* **17** 3175 (2007).
130. J-H Kim, A Manthiram *J. Electrochem. Soc.* **155** B385 (2008)
131. J-H Kim, F Prado, A Manthiram *J. Electrochem. Soc.* **155** B1023 (2008)
132. S Ya Istomin, J Grins, G Svensson, O A Drozhzhin, V L Kozhevnikov, E V Antipov, J P Attfield *Chem. Mater.* **15** 4012 (2003)
133. S Ya Istomin, O A Drozhzhin, G Svensson, E V Antipov *Solid State Sci.* **6** 539 (2004)
134. D Rupasov, A Chroneos, D Parfitt, J A Kilner, R W Grimes, S Ya Istomin, E V Antipov *Phys. Rev. B: Condens. Matter* **79** 172102 (2009)
135. Y Li, Y N Kim, J Cheng, J A Alonso, Z Hu, Y-Y Chin, T Takami, M T Fernández-Díaz, H-J Lin, C-T Chen, L H Tjeng, A Manthiram, J B Goodenough *Chem. Mater.* **23** 5037 (2011)
136. T Liu, Y Li, J B Goodenough *J. Power Sources* **199** 161 (2012)
137. D V Sheptyakov, V Yu Pomjakushin, O A Drozhzhin, S Ya Istomin, E V Antipov, I A Bobrikov, A M Balagurov *Phys. Rev. B: Condens. Matter* **80** 024409 (2009)
138. Ph S Napolsky, O A Drozhzhin, S Ya Istomin, S M Kazakov, E V Antipov, A V Galeeva, A A Gippius, G Svensson, A M Abakumov, G van Tendeloo *J. Solid State Chem.* **192** 186 (2012)
139. I Burmistrov, O A Drozhzhin, S Ya Istomin, V V Sinitsyn, E V Antipov, S I Bredikhin *J. Electrochem. Soc.* **156** B1212 (2009)
140. O A Drozhzhin, F S Napol'skii, S Ya Istomin, E V Antipov *Moscow Univ. Chem. Bull.* **62** 167 (2007)
141. E Boehm, J-M Bassat, P Dordor, F Mauvy, J-C Grenier, Ph Stevens *Solid State Ionics* **176** 2717 (2005)
142. C Allanion, P Odier, J M Bassat, J P Loup *J. Solid State Chem.* **131** 167 (1997)
143. D J Buttrey, P Ganguly, J M Honig, C N R Rao, R R Schartman, G N Subanna *J. Solid State Chem.* **74** 233 (1988)
144. A Chroneos, D Parfitt, J A Kilner, R W Grimes *J. Mater. Chem.* **20** 266 (2010)
145. C Allanyon, J Rodríguez-Carvajal, M T Fernandez-Díaz, P Odier, J M Bassat, J P Loup, J L Martínez *Z. Phys. B: Condens. Matter* **100** 85 (1996)
146. C Ferchaud, J-C Grenier, Y Zhang-Steenwinkel, M M A van Tuel, F P F van Berkel, J-M Bassat *J. Power Sources* **196** 1872 (2011)
147. S Nishimoto, S Takashi, Y Kameshima, M Matsuda, M Miyake *J. Ceram. Soc. Jpn.* **119** 246 (2011)
148. J Wan, J B Goodenough, J H Zhu *Solid State Ionics* **178** 281 (2007)
149. P Odier, Ch Allanion, J M Bassat *J. Solid State Chem.* **153** 381 (2000)
150. F Mauvy, C Lalanne, J-M Bassat, J-C Grenier, H Zhao, L Huo, Ph Stevens *J. Electrochem. Soc.* **153** A1547 (2006)
151. A Montenegro-Hernandez, J Vega-Castillo, L Mogni, A Caneiro *Int. J. Hydrogen Energy* **36** 15704 (2011)
152. A George, I Gopalakrishnan, M Karkhanavala *Mater. Res. Bull.* **9** 721 (1974)
153. Y Tokura, K Kikuchi, T Arima *Phys. Rev. B: Condens. Matter* **45** 7580 (1992)
154. G N Mazo, Yu A Mamaev, M Ts Galin, M S Kaluzhskikh, A K Ivanov-Schitts, E V Antipov *Inorg. Mater.* **47** 1218 (2011)
155. N V Lyskov, M S Kaluzhskikh, L S Leonova, G N Mazo, S Ya Istomin, E V Antipov *Int. J. Hydrogen Energy* **37** 18357 (2012)
156. K Zheng, A Gorzkowska-Sobas, K Swierczek *Mater. Res. Bull.* **47** 4089 (2012)

[a] — *Crstallogr. Rep. (Engl. Transl.)*